Supporting Information for

A river on fiber: high resolution fluvial monitoring with distributed acoustic sensing

Danica L. Roth[1*], Maximiliano J. Bezada[2], Ge Jin[3], Claire C. Masteller[4], Matthew R. Siegfried[3,5], Aleksei Titov[3], Bill Tate[2]

[1]Cooperative Institute for Research In Environmental Sciences, University of Colorado, Boulder, CO, USA.

[2]Earth & Environmental Sciences, University of Minnesota, Minneapolis, MN, USA.

[3]Department of Geophysics, Colorado School of Mines, Golden, CO, USA.

[4]Earth, Environmental, and Planetary Sciences, Washington University in St. Louis, St. Louis, MO, USA.

[5]Hydrologic Science & Engineering Program, Colorado School of Mines, Golden, CO, USA.

[*]Corresponding author: danica.roth@colorado.edu, ORCID ID: 0000-0001-9502-7836

Contents of this file

Figures S1 to S8
Text S1 to S3

Introduction

This Supporting Information includes supplemental figures and text that provide additional context for the analyses presented in the main manuscript. The figures include full-scale deployment photographs; spatial spectrograms and along-cable wave correlation; an image and caption representative of the supplemental audio-spectral movie; example high-frequency spectra illustrating instrument response; sample microstrain-rate waveforms showing impulsive signals and reflections; and unnormalized data and model spectrograms demonstrating spatial gliding from impulse reflections. The supplemental text provides details of the Shields stress calculations and quantitative examples exploring potential mechanisms for spatial gliding, including resonance in a thinning alluvial layer and Helmholtz or cavity resonance within pore spaces between cobbles.

Figure S1. Full size photograph of tap test and DAS cable along cement reinforced bank next to uppermost rapids.

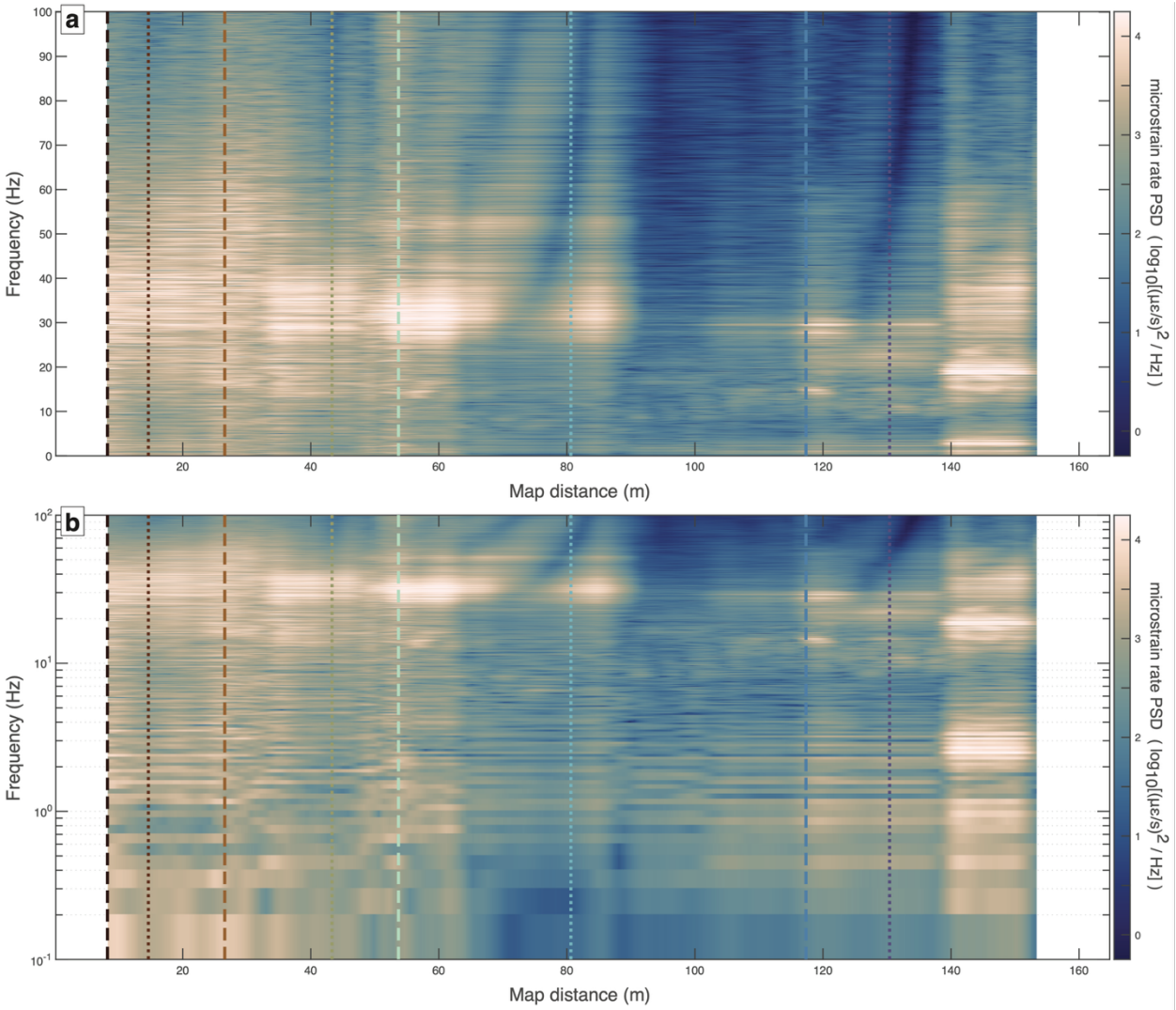

Figure S2. Spatial spectrograms showing power spectral density (PSD) averaged over three 10 s segments of microstrain rate data at each position. Spectrograms shown up to 100 Hz on both **a)** linear and **b)** log frequency axes. Vertical dashed and dotted lines indicate locations of example spectra shown in Figures 3 and S6.

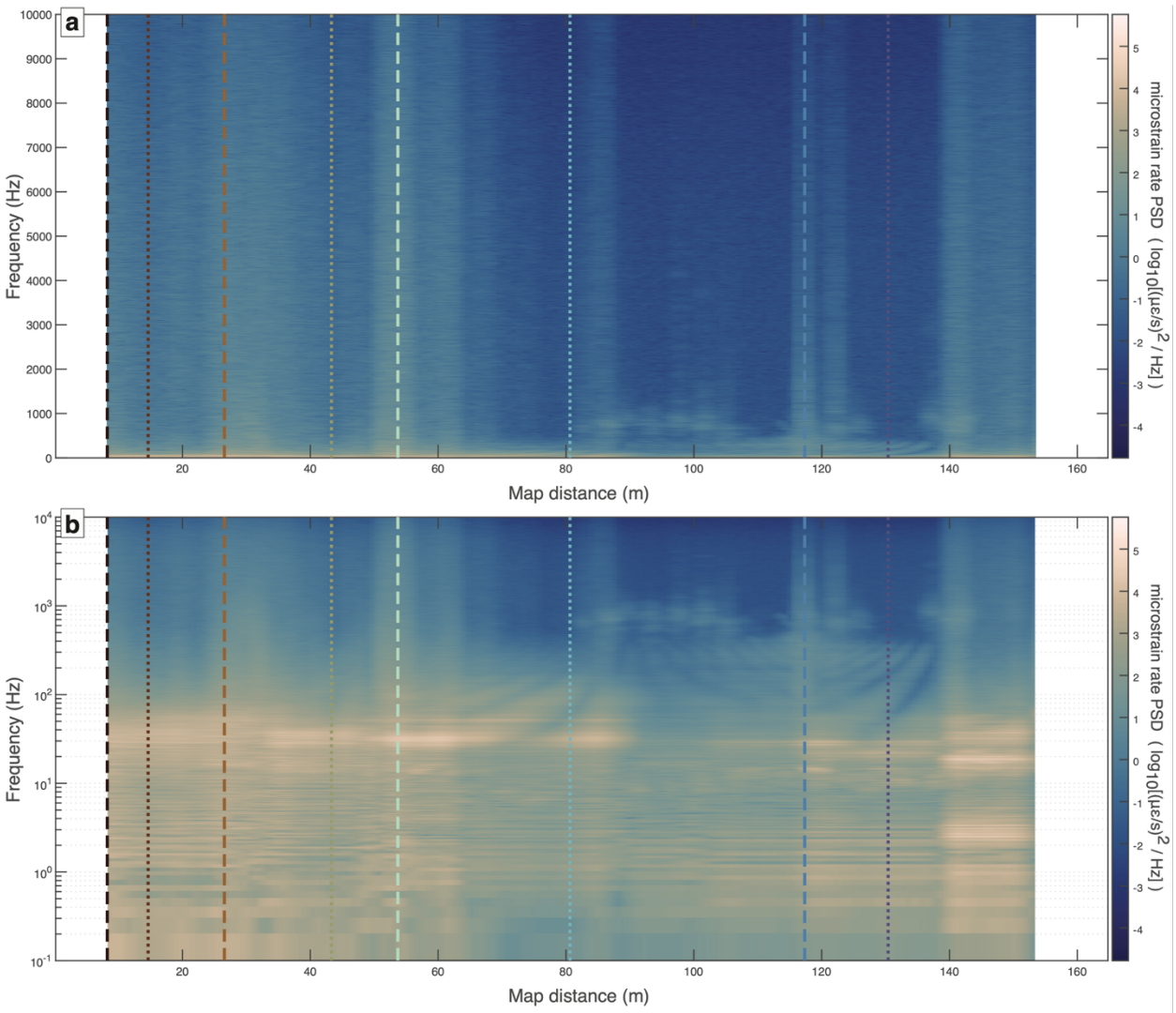

Figure S3. Spatial spectrograms showing power spectral density (PSD) averaged over three 10 s segments of microstrain rate data at each position. Spectrograms shown up to 10 kHz on both **a)** linear and **b)** log frequency axes over full range of PSD values. Vertical dashed and dotted lines indicate locations of example spectra shown in Figures 3 and S6.

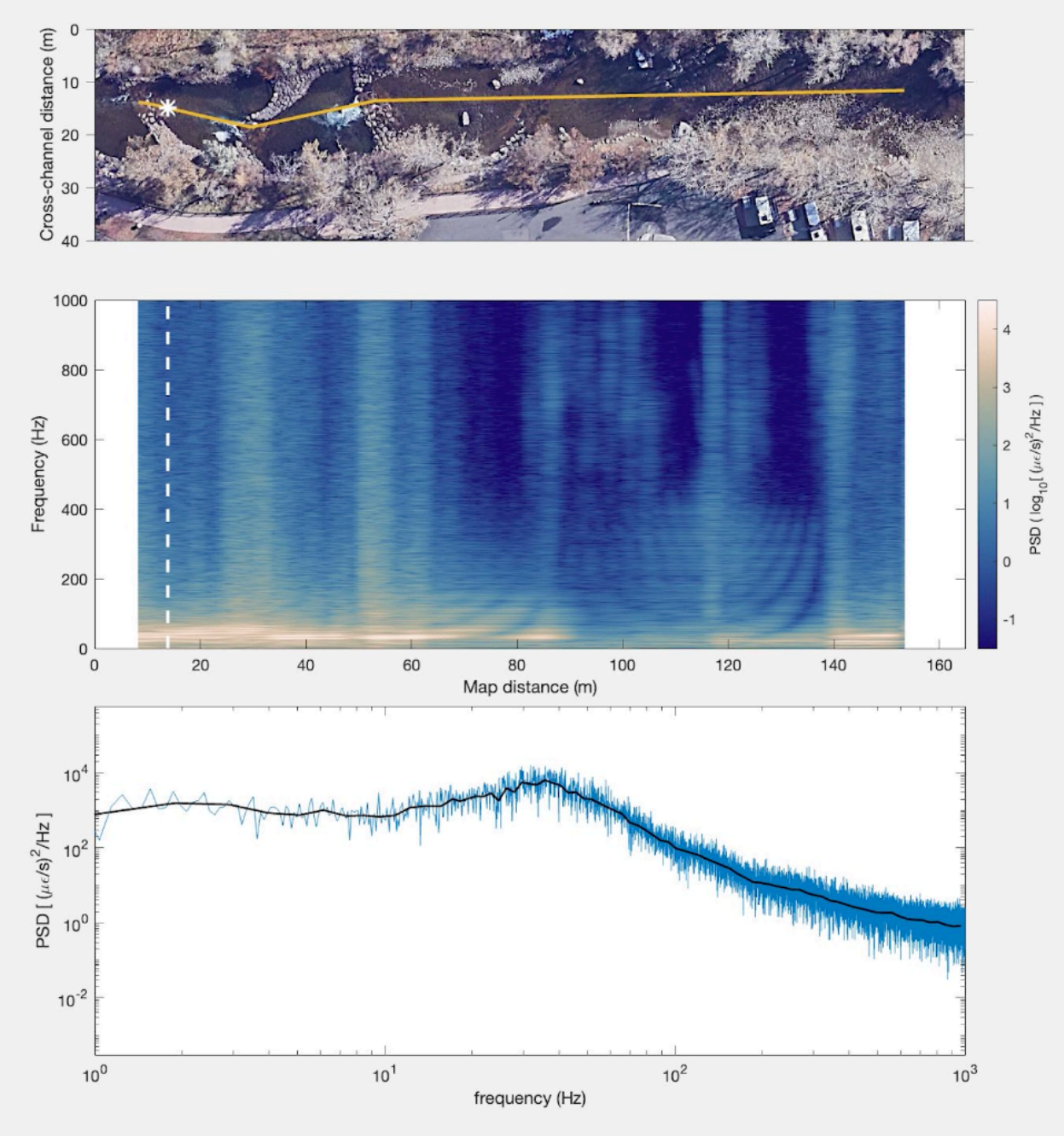

Figure S4. (Caption for Supplemental Movie) Movie of DAS audio-spectral soundscape along the creek. The DAS power spectrum and 0.3 s of accompanying audio from each DAS channel along the creek. Channel locations indicated by moving white asterisk in top panel and vertical white dashed line in central panel.

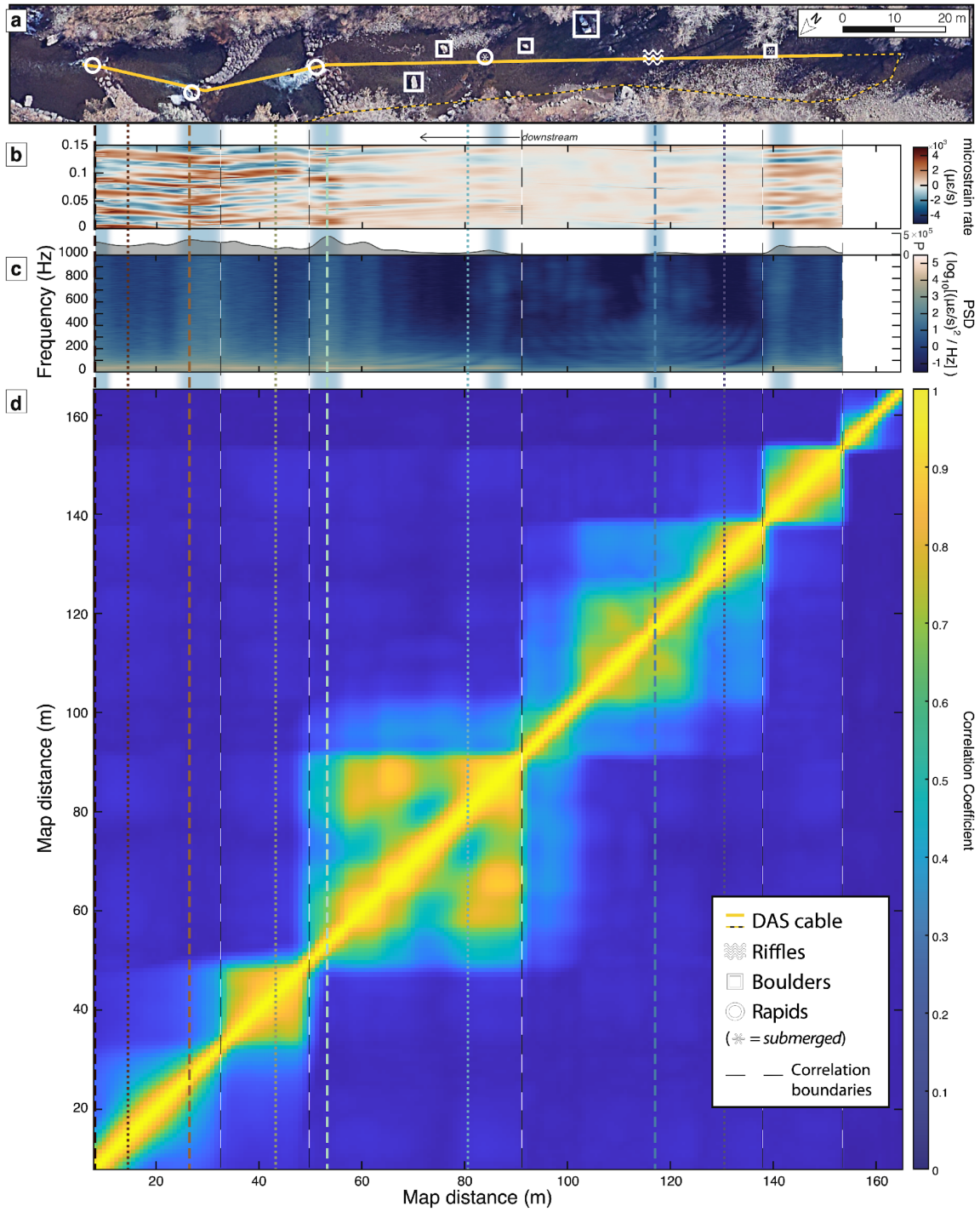

Figure S5. All spatially aligned DAS data from Figures 1 and 2 (main text), shown together for ease of spatial referencing. **a)** Site map, **b)** microstrain rate, **c)** power spectral density (PSD) and total signal power (P) (gray) (shown in Figure 1), and **d)** along-stream wave coherence (shown in Figure 2). Vertical dashed and dotted lines indicate locations of example spectra shown in Figures 3 and S6; long dashed lines mark approximate boundaries between regions of high coherence.

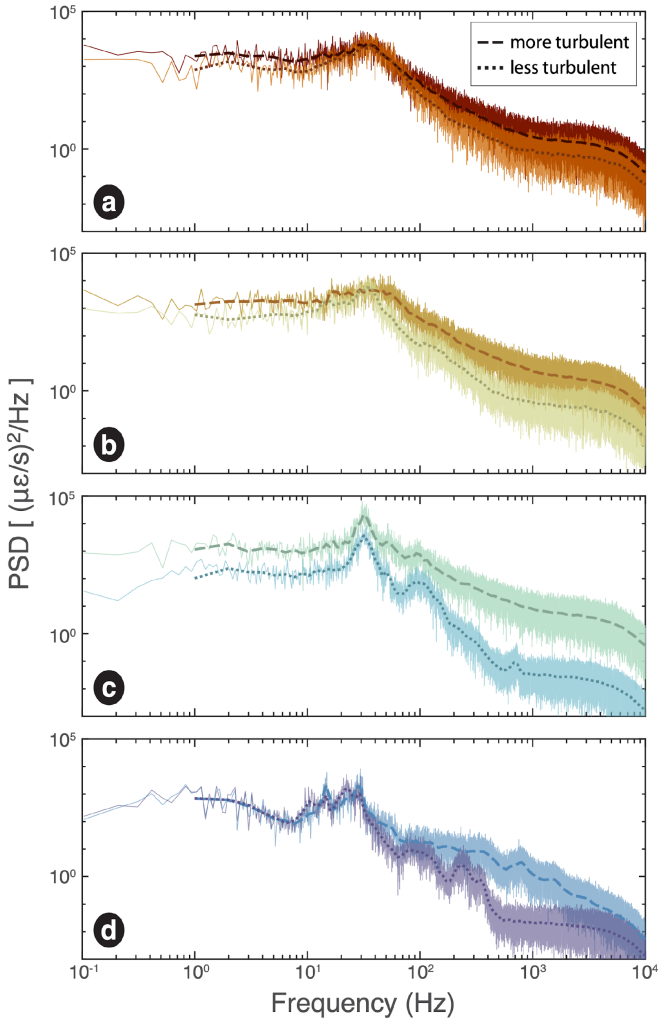

Figure S6. Example power spectra comparing broadband signals (dashed lines) from regions with enhanced turbulence and neighboring regions (dotted lines) with less turbulent flow across entire frequency range recorded by DAS. Line colors correspond with Figure 1 and central lines show log-binned average power density for each spectrum. Starting at the downstream end of the study reach, spectra show **a-c)** the three rapids and pools immediately upstream of each rapid, and **d)** the run-riffle sequence upstream. Note that ~4 kHz appears to be a corner above which frequency response declines systematically, assumed to represent an instrument limitation. This frequency range is therefore not shown in the main text.

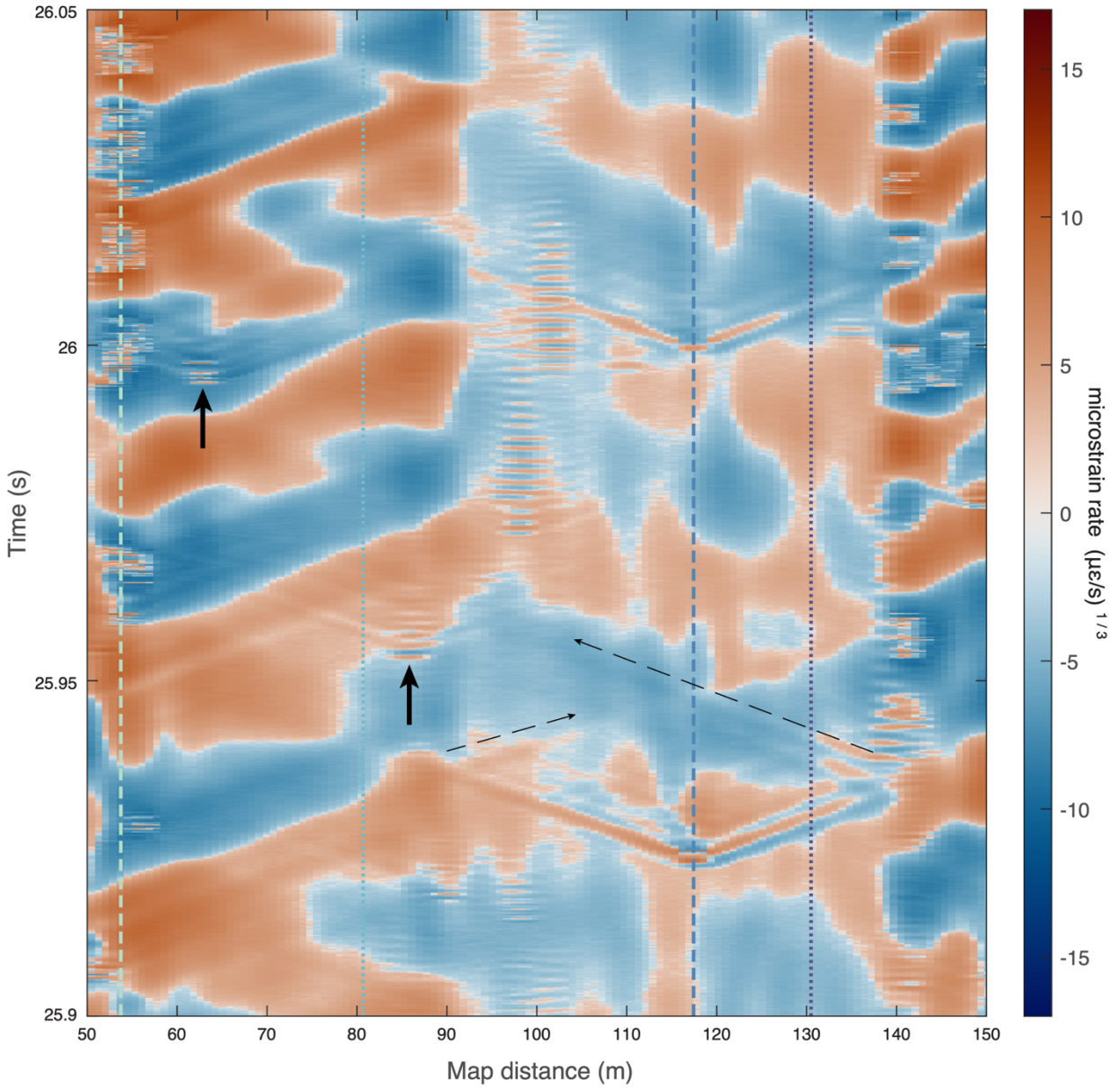

Figure S7. Example microstrain rate showing two "knocking" impulses with reflections and other impulsive phenomena. The impulse at ~25.925 s and ~117 m map distance produces reflections at map distances of ~90 m and ~140 m (below dashed black arrows), whereas impulse at ~26 s only a reflection at ~140 m. Solid black arrows point to other potential impulsive sources at ~85 m (approximate location of submerged rapid) and ~62 m (entering the uppermost major rapid), where the cable may also have occasionally interacted with the cemented boulder bed. Vertical dashed and dotted lines indicate locations of example spectra shown in Figures 3 and S6.

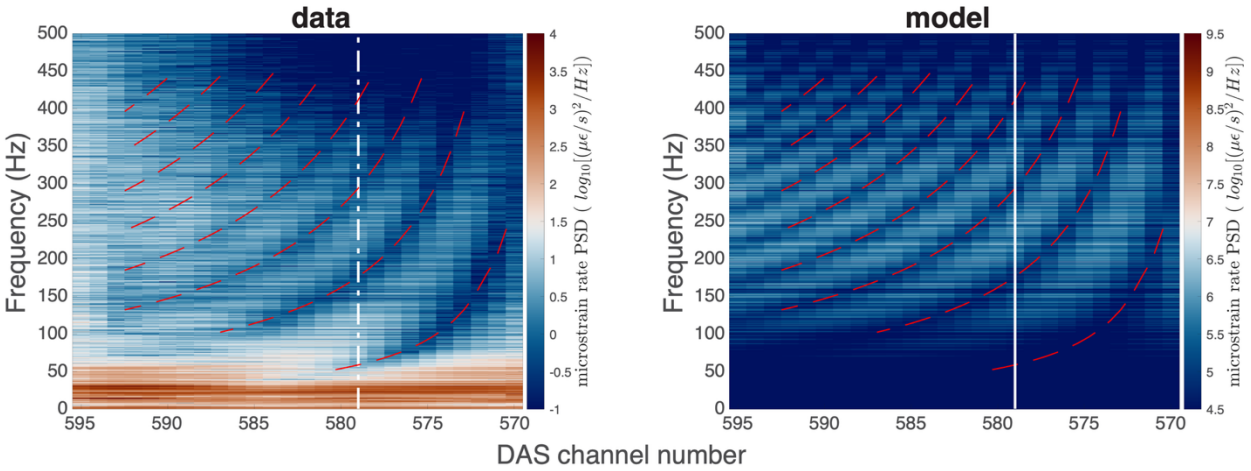

Figure S8. Observed and modeled spatial spectrograms of power spectral density (PSD) (shown on adjusted color scale relative to Fig. 1 to improve visibility), annotated with red dashed lines showing observed bandgaps traced from the DAS spectrogram. Channel 579 is indicated by the white lines in part (b), and is the same channel shown in Fig. 3d.

S1. Shields stress

We used river flow depths collected concurrent with DAS deployment to estimate the riverbed shear stress and the associated potential for grain motion. We calculated a dimensionless Shields stress, τ^*, criteria, which approximates the ratio of driving and resisting stresses acting on a particle as,

$$\tau^* = \frac{\rho h S}{(\rho_s - \rho) D_{50}}, \quad (1)$$

where ρ is the fluid density (kg/m^3), ρ_s is the sediment density (kg/m^3), h is flow depth (m), S is the bed slope (m/m), and D_{50} is the median grain size of particles on the riverbed (m). It is generally accepted that the threshold for particle transport, often called critical Shields stress, τ_c^*, is well-described by a narrow range of Shields stress values, τ_c^* = 0.03 – 0.08 (Buffington and Montgomery, 1997). We thus computed a range of Shields stresses during deployment as a fraction of τ_c^* by solving Eq. 1 using an assumed sediment density of ρ_s = 2700 kg/m^3 and measured channel bed slope (S = 0.003), median grain size (D_{50}= 0.05 m) and minimum and maximum surveyed thalweg flow depths (h = 0.21 – 0.55 m) in the study reach. Estimated τ^* / τ_c^* during deployment fell between 9.3% (for τ_c^* = 0.08) and 64.7% (for τ_c^* = 0.03), indicating that shear stress was well below typical values required to initiate sediment movement.

S2. Resonance in a thinning alluvial layer

We estimate the fundamental frequency $f_r = v_s/4Z$ for a simplified two-layer system composed of bedrock overlain by a lower-impedance alluvium layer with thickness Z and mean shear wave velocity v_s (Ibs-von Seht & Wohlenberg, 1999; Anthony et al, 2018). Assuming a ~2 m thick sediment layer near the riffle center, the ~ 40 Hz fundamental frequency observed here would correspond with a shear velocity around ~320 m/s, consistent with reported values for unconsolidated, water-rich surface sediments (Wang et al., 2022). Using this velocity, the ~ 350 Hz peak observed upstream of the riffle would indicate thinning of the alluvial layer to ~0.23 m. We cannot evaluate the validity of these estimates because we lack direct measurements of alluvial thickness during the deployment, and the pulse-train hypothesis examined in section 5.3 more parsimoniously explains the observed spatio-spectral gliding. Nonetheless, this example demonstrates that resonance in a gravel layer provides a physically plausible mechanism for spatio-spectral gliding.

S3. Helmholtz or cavity resonance in pore spaces between cobbles

Self-sustained harmonic oscillations can also arise from shear flow over boundaries of varying geometries (Rockwell and Naudascher, 1979), a process previously documented in association with laboratory flows (Rockwell and Naudascher, 1979; Chanaud and Powell, 1965; Howe, 1998), volcanic gas jets (Matoza et al., 2010) and asphalt or pavement (Ohiduzzaman et al., 2016). The fundamental frequency f_r associated with Helmholtz resonance can be estimated as $f_r = \frac{c}{2\pi}\sqrt{\frac{A}{LV}}$, where c is the acoustic wavespeed in water, L is a corrected length of the neck providing entry into the cavity, A is the surface area of the neck opening and V is the volume of the cavity. If Helmholtz resonance in the pore spaces between cobbles was responsible for the spatio-spectral gliding found in this study, the observed increase in lowest frequency mode from ~40 Hz to ~350 Hz upstream of the riffle would require the ratio $\frac{A}{LV}$ to increase by a factor of ~76, implying strong spatial variability in pore geometry.